JOURNAL OF GEOPHYSICAL RESEARCH, VOL. 107, NO. D20, 8036, DOI 10.1029/2001JD900216, 2002

Regional simulation of interannual variability over South America

V. Misra, P. A. Dirmeyer, and B. P. Kirtman

Center for Ocean-Land-Atmosphere Studies, Institute of Global Environment and Society, Inc., Calverton, Maryland, USA

H.-M. Henry Juang

National Centers for Environmental Prediction, Climate Prediction Center, Camp Springs, Maryland, USA

M. Kanamitsu

Climate research Division, Scripps Institution of Oceanography, University of California, San Diego, La Jolla, California, USA

Received 29 September 2000; revised 22 March 2001; accepted 9 April 2001; published 22 August 2002.

[1] Three regional climate simulations covering the austral summer season during three contrasting phases of the El Niño-Southern Oscillation cycle were conducted with the Regional Spectral Model (RSM) developed at the National Centers for Environmental Prediction (NCEP). The simulated interannual variability of precipitation over the Amazon River Basin, the Intertropical Convergence Zone, the Pacific and Atlantic Ocean basins, and extratropical South America compare reasonably well with observations. The RSM optimally filters the peturbations about a time-varying base field, thereby enhancing the information content of the global NCEP reanalysis. The model is better than the reanalysis in reproducing the observed interannual variability of outgoing longwave radiation at both high frequencies (3–30 days) and intraseasonal (30–60 days) scales. The low-level jet shows a peak in its speed in 1998 and a minimum in the 1999 simulations. The lag correlation of the jet index with convection over various areas in continental South America indicates that the jet induces precipitation over the Pampas region downstream. A detailed moisture budget was conducted over various subregions. This budget reveals that moisture flux convergence determines most of the interannual variability of precipitation over the Amazon Basin, the Atlantic Intertropical Convergence Zone, and the Nordeste region of Brazil. However, both surface evaporation and surface moisture flux convergence were found to be critical in determining the interannual variability of precipitation over the southern Pampas, Gran Chaco area, and the South Atlantic Convergence Zone. *INDEX TERMS:* 3309 Meteorology and Atmospheric Dynamics: Climatology (1620); 1836 Hydrology: Hydrologic budget (1655); 3374 Meteorology and Atmospheric Dynamics: Tropical meteorology; 3354 Meteorology and Atmospheric Dynamics: Precipitation (1854); 9360 Information Related to Geographic Region: South America *KEYWORDS:* South America, low-level jet, interannual variability, regional climate, moisture budget.

1. Introduction

[2] Many observational studies have shown a robust relationship between rainfall at regional scales over South America and the global scale phenomenon of El Niño and the Southern Oscillation (ENSO) [*Ropelewski and Halpert*, 1987]. Likewise, such a synergy has been observed between the Atlantic sea surface temperature (SST) and rainfall anomalies over the Nordeste region [*Uvo et al.*, 1998; *Nobre and Shukla*, 1996]. Using rain guage measurements from 105 stations, *Uvo et al.* [1998] showed a negative (positive) relationship between the seasonal mean precipitation over Nordeste and the SST anomalies in the Pacific (South Atlantic) during E1 Niño years. Furthermore, they find that the Pacific correlations were weaker than the Atlantic correlations. From an analysis of data sets incorporating a global precipitation index, rain guage observations and National Aeronautics and Space Agency/Data Assimilation Office four-dimensional (4-D) analysis, *Lenters and Cook* [1999] found that the Altiplano plateau to the east of the Andes has drier conditions and there is a northward shift of the Bolivian high during El Niño years. In the extratropics, *Pisciottano et al.* [1994] showed a positive correlation between observed monthly precipitation reported over Uruguay and El Niño SST anomalies over the Pacific. However, they also provided evidence of spatial and temporal asymmetries, such as the disappearance and reversal of the sign of the rainfall anomalies after La Niña years over southern Uruguay. *Grimm et al.* [2000] found a near-linear behavior of rainfall anomalies in a number of regions in southern South America in response to tropical SST anomalies.

[3] It is evident from the above discussion that the summer season precipitation over South America exhibits pronounced spatial and temporal variability. Within the austral summer season the movements of the South Atlantic Convergence

Copyright 2002 by the American Geophysical Union.
0148-0227/02/2001JD900216$09.00

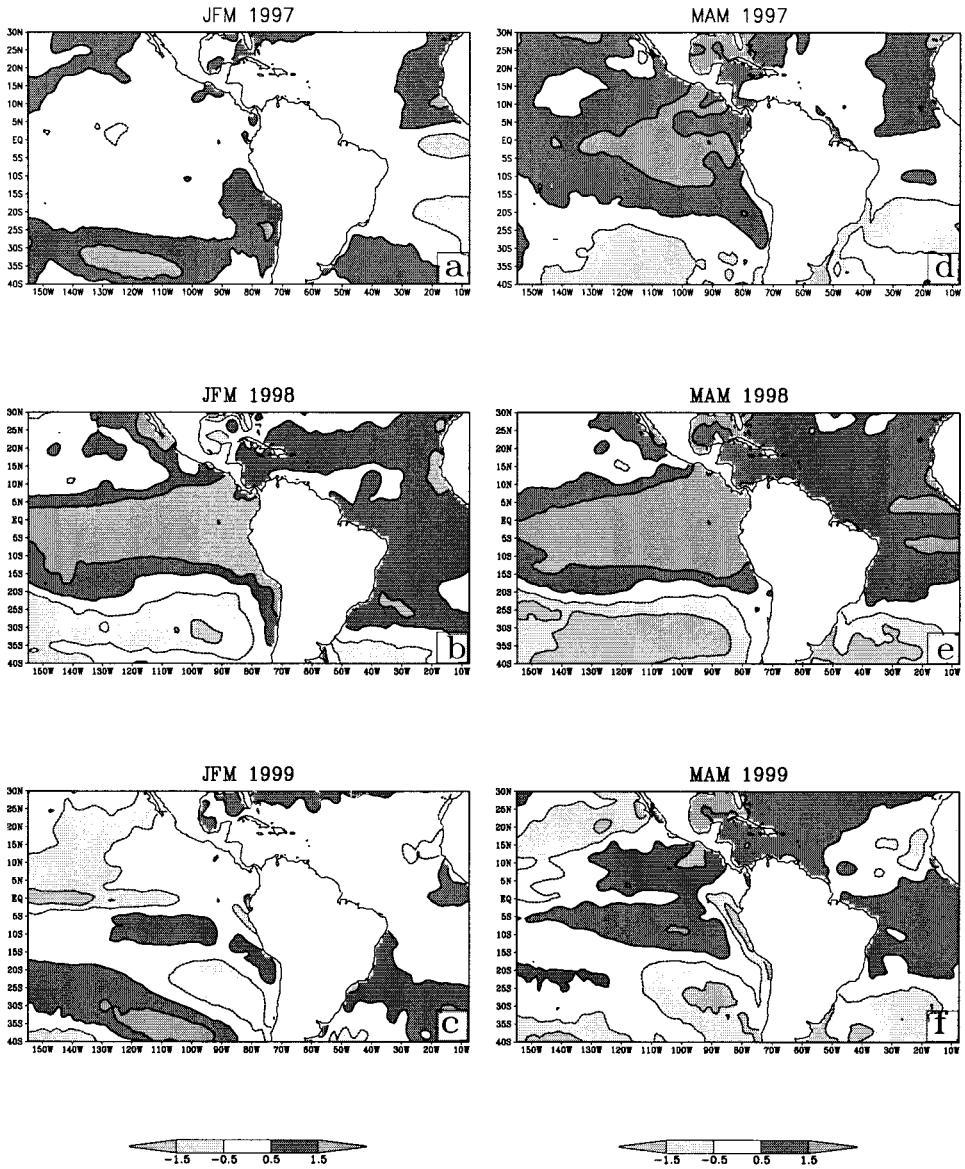

Figure 1. Seasonally averaged sea surface temperature anomalies for January-February-March of (a) 1997, (b) 1998, and (c) 1999 and March-April-May of (e) 1997, (f) 1998, and (g) 1999. Units are in °C.

Zone (SACZ), South Atlantic subtropical high (SASH), and the Bolivian high (BH) along with the intrusion of cold fronts from the extratropics hold significant ramifications for the interannual variability of the regional climate in the area. *Paegle and Mo* [1997] show that when the SACZ is intense, the SASH moves eastward and diminishes the northerly (vertically integrated) moisture flux into the Amazon Basin resulting in dry spells of the austral summer season over the region. *Liebmann et al.* [1999], while examining the variance of outgoing longwave radiation, showed that the south central Amazon exhibited a large subseasonal variance relative to the interannual variance. The very high frequency (3–30 days) convective activity was restricted to the area over the central Amazon. The interannual variation of this intraseasonal variability is investigated further in this study.

[4] Figure 1 displays the seasonal mean SST anomalies for the January-February-March (JFM) and March-April-May (MAM) seasons of 1997, 1998, and 1999. The SST anomalies are derived from the weekly optimally interpolated (OI) SST of *Reynolds and Smith* [1994]. The anomalous warm temperatures in the central and eastern Pacific near the equator in 1998 are evident in Figures 1b and 1e. Similarly, the relatively cooler SST of 1999 over the equatorial Pacific region is obvious in Figures 1c and 1f. However, it should be mentioned that 1999 was a rather weak La Niña event with negative anomalies over the far eastern Pacific weakening slightly from JFM to MAM, although the negative SST anomalies off the coast of Peru and subtropical South Pacific strengthen from JFM (Figure 1c) to MAM (Figure 1f).

[5] In this study we examine the simulation of the interannual variability of the rainfall and circulation features during austral summer season over tropical and extratropical South America and the tropical Pacific and Atlantic Ocean basins from a high-resolution regional climate model. The austral summer seasons of 1997, 1998, and 1999 are analyzed to begin to understand the regional climate variations over this region under the influence of strong interannual variability of SST.

[6] The South American region has a complex terrain, steep topography and large land surface heterogeneity. Fur-

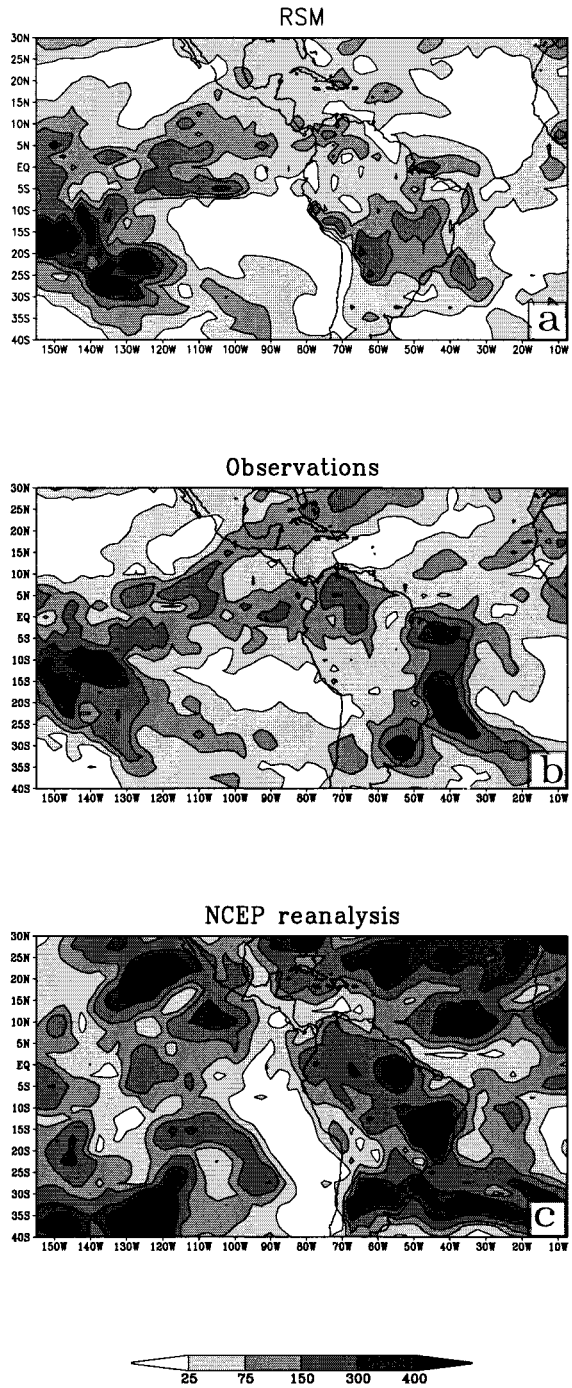

Figure 2. January-February-March variance of outgoing longwave radiation at 30–60 days (intraseasonal) scale from (a) RSM, (b) observations, and (c) NCEP reanalysis in 1998. The units are in W^2/m^4.

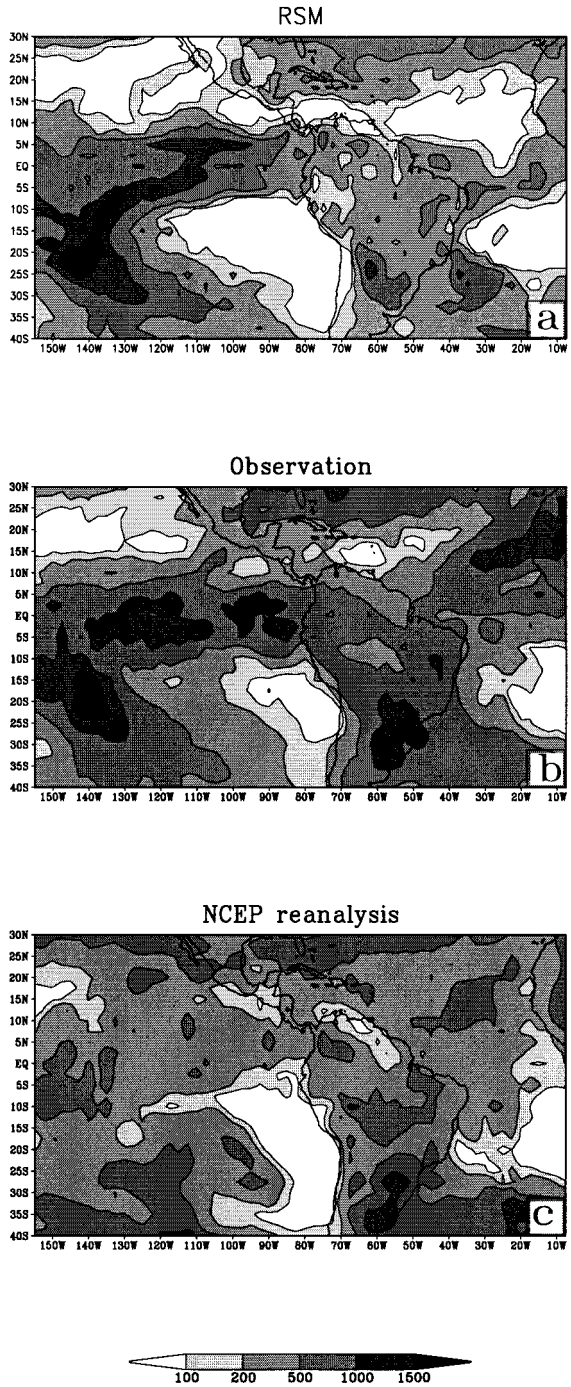

Figure 3. The January-February-March variance of outgoing longwave radiation at 3–30 days scale (high frequency) from (a) RSM, (b) Observations and (c) NCEP reanalysis in 1998. The units are in W^2/m^4.

thermore, it is an area that is strongly influenced by the Intertropical Convergence Zone (ITCZ), the South Atlantic Convergence Zone (SACZ), and deep convection over the central Amazon, resulting in a great deal of mesoscale structure and strong gradients of rainfall over the region. *Mohr and Zipser* [1996] have shown from satellite measurements that tropical South America is one of the most active centers of mesoscale convective systems. Since the coupled general circulation models have too coarse a resolution to resolve these fine scale features, we use a relatively high-resolution regional climate modeling.

[7] This research is a prelude to the development of a high-resolution regional climate prediction system driven by a general circulation model (coupled to the ocean and land surface processes). Here we shall examine the skill of the regional atmospheric model in simulating the variability of the regional climate during normal (1997), El Niño (1998), and La Niña (1999) years.

[8] In the following section a brief description of the model

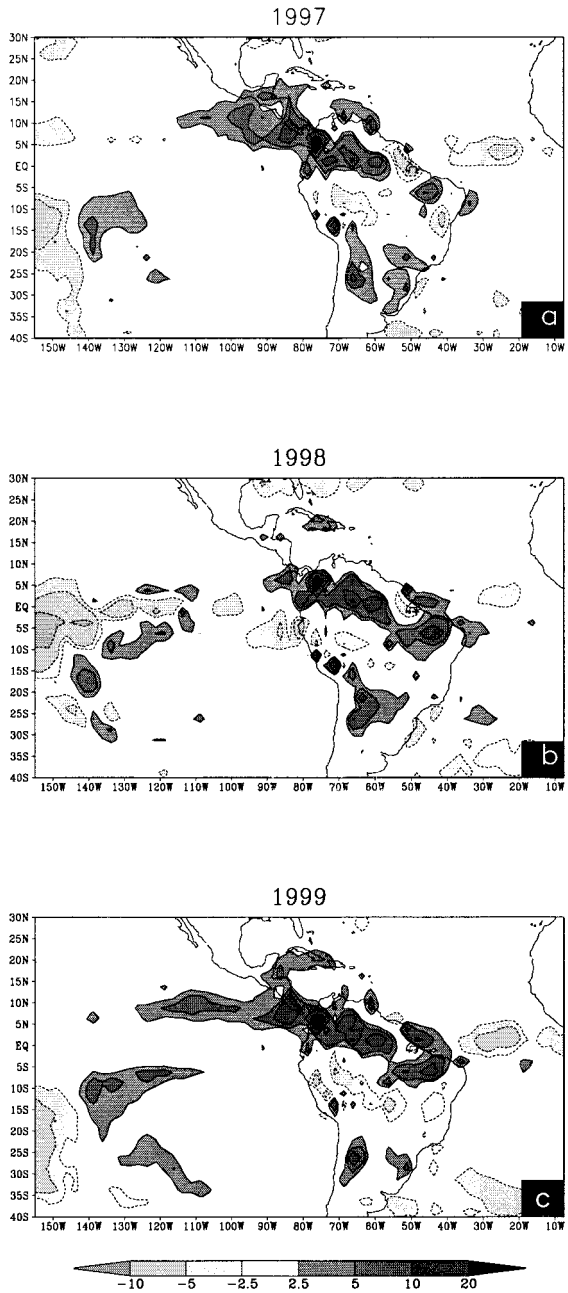

Figure 4. Seasonal (JFM) precipitation errors of the Regional Spectral Model in (a) 1997, (b) 1998, and (c) 1999. The units are in mm/d.

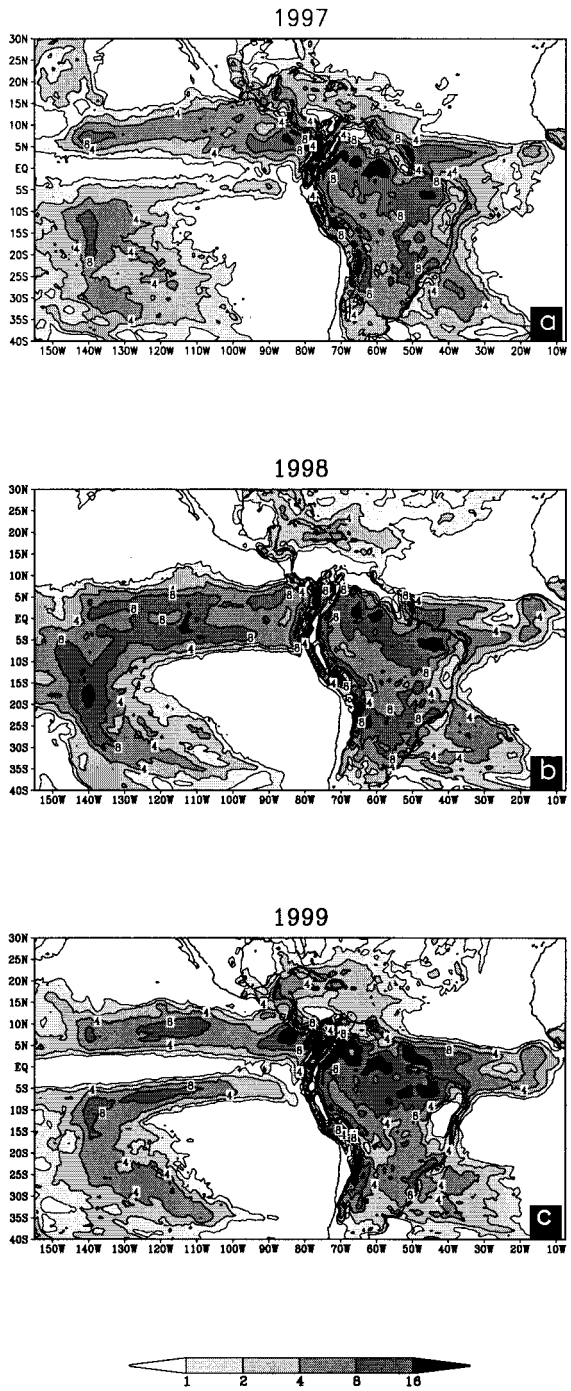

Figure 5. Seasonal precipitation (JFM) from the Regional Spectral Model in (a) 1997, (b) 1998, and (c) 1999. The units are in mm/d.

is given. More details of the model can be found in the works of *Juang and Kanamitsu* [1994] and *Juang et al.* [1997]. In section 3 we discuss the model results, followed by conclusions in section 4.

2. Model Description

[9] We have adopted the Regional Spectral Model (RSM) developed by *Juang and Kanamitsu* [1994] and *Juang et al.* [1997] for our seasonal simulation runs. The RSM predicts the total variable from which it determines the perturbations about the time-varying global field (in this case National Center for Environmental Protection (NCEP) reanalysis) in the regional domain. These perturbations are then smoothly relaxed to zero at the lateral boundaries in grid space and then Fourier transformed to satisfy solid wall (or symmetric) boundary conditions.

[10] The RSM uses the terrain following sigma coordinate in the vertical with 28 levels. In the vertical, a second-order central finite difference formulation is used. The model equations are integrated by a semi-implicit scheme. The humidity equation is integrated explicitly.

[11] The model has a comprehensive physics package that

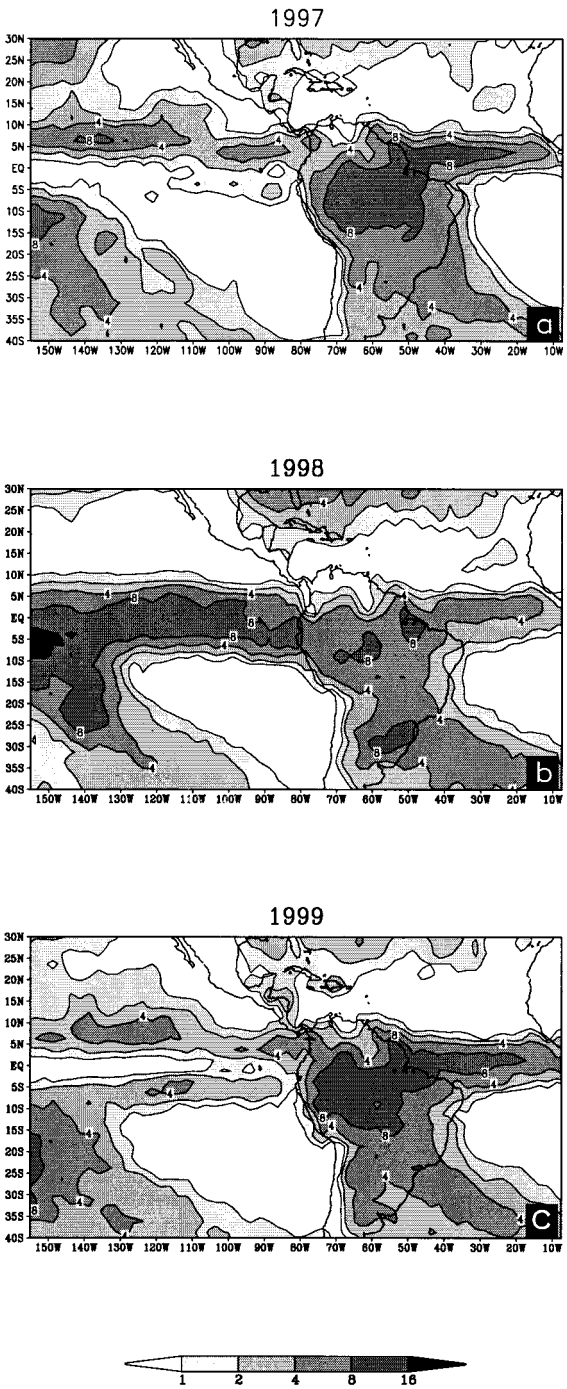

Figure 6. Seasonal precipitation (JFM) from observations [*Xie and Arkin*, 1996] for (a) 1997, (b) 1998, and (c) 1999. The units are in mm/d.

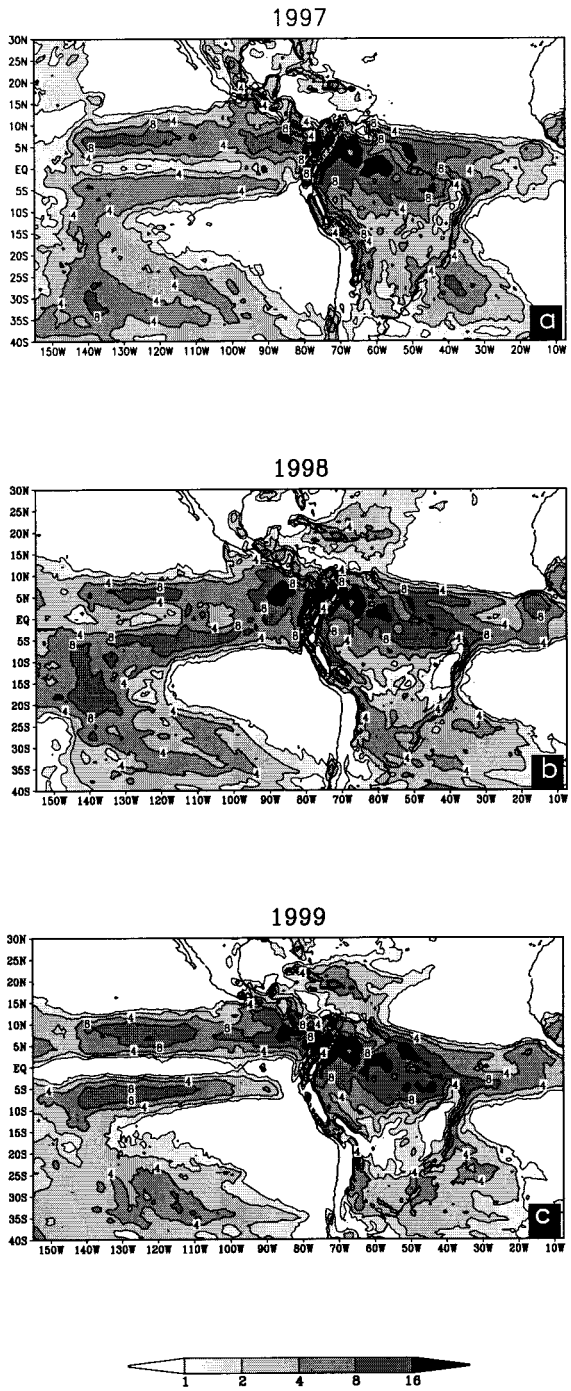

Figure 7. Same as Figure 5 but for the MAM season.

includes shortwave [*Chou*, 1992] and longwave [*Fels and Schwarzkopf*, 1975] radiation which are fully interactive with the clouds. The boundary layer physics in the model employs a nonlocal diffusion scheme developed by *Hong and Pan* [1996] which is strongly coupled to the surface layer physics. The flux computations in the surface layer are based on Monin-Obukhov similarity theory. The model also includes a two-layer soil model of *Mahrt and Pan* [1984], *Pan and Mahrt* [1987], and *Pan* [1990]. The deep convection in the model is parameterized with a simplified Arakawa-Schubert scheme [*Pan and Wu*, 1995]. The large-scale condensation (and re-evaporation) involves disposition of supersaturation. Shallow convection following *Tiedtke* [1984] is invoked only in the absence of deep convection. The gravity wave drag formulation of *Alpert et al.* [1988] is also included.

[12] In this study the RSM is at an 80 km grid resolution with dimensions of 217×112 centered at 15°S and 80°W. The time step of integration is 240 s. The NCEP reanalysis (on a Gaussian grid of triangular truncation at wave number 62) provides the time-dependent base field, which is updated every 12 hours. The base field is linearly interpolated in time and bicubic spline interpolated in space to the RSM grid.

Time-varying SST and sea ice are prescribed in the integration. They are updated daily by linearly interpolating from weekly *Reynolds and Smith* [1994] optimum interpolation SST data set. The snow cover and soil moisture are prescribed initially from NCEP reanalysis but predicted thereafter. The integrations for each year start with NCEP reanalysis from 0000 UTC 13 December and end on 0000 UTC 1 June.

3. Results

[13] The model results have been analyzed for both the JFM and the MAM seasons. However, when the results are nearly the same for both seasons, we shall restrict our discussion to one of them. The 1998 and 1999 simulations are used to highlight the interannual variation.

3.1. Outgoing Longwave Radiation

[14] The simulated outgoing longwave radiation (OLR) is compared to observations of *Liebmann and Smith* [1996]. The OLR is used for validation because the observations are completely independent. The observed OLR is available daily on a 2.5° grid. The corresponding NCEP reanalysis of OLR is shown to assess the impact of the relatively higher resolution of the RSM. Both intraseasonal and high frequencies are compared. A spectral band-pass filter is employed on the model output and observations to obtain the high (3–30 days) and intraseasonal (30–60 days) frequencies. *Liebmann et al.* [1999] have indicated the importance of the subseasonal anomalies (from observed OLR) propagating from the SACZ, which define episodes of dry and wet events over southern Brazil. In the subsequent section the seasonal precipitation errors of the RSM are dicussed. It should be noted that both the RSM output and the NCEP reanalysis were interpolated to the observational grid for these comparisons.

3.1.1. Intraseasonal Variability

[15] Figures 2a–2c show the variance of OLR on intraseasonal (30–60 days) time scales from the RSM, observations, and NCEP reanalysis for 1998. There is a distinct improvement in RSM compared to NCEP reanalysis over both the Pacific and the Atlantic Ocean basins. The large variance observed over the Pacific Ocean at 10°S–20°S and 150°W–130°W and its northeastward and southeastward extensions (Figure 2b) is captured by the RSM (Figure 2a). So is the low-variance region over the equatorial Atlantic where the NCEP reanalysis (Figure 2c) has erroneously a large variance of over 400 W^2/m^4. However, over continental South America the performance is not so encouraging. The variance over land simulated by RSM in Figure 2a is far less than in the observations (Figure 2b) and in the NCEP reanalysis. However, there are areas over land where RSM shows improvement over the NCEP reanalysis, such as over the Llanos and the Pakaraima Mountains in northern Brazil where RSM captures the region of high-variance, albeit less than the observations. Similarly, the structure of the high variance region depicted by the 75 W^2/m^4 contour extending from northwest Brazil into the Atlantic Ocean in the RSM simulation (Figure 2a) can be seen as a improvement over NCEP reanalysis (Figure 2c) in comparison to the observations. The variance maxima in the NCEP reanalysis (Figure 2c) over land are systematically displaced to the west compared to observations. During 1999 (not shown) the RSM continues to show an improvement over the Pacific and Atlantic Ocean basins. However, over land, particularly over the SACZ region, the RSM predicts a smaller variance than observations and NCEP reanalysis. We suspect this consistent shortcoming of the RSM over this region at both high frequency and intraseasonal scales may be due in part to the inability of the model to simulate the cold front intrusions from the midlatitudes due to the constraint at the lateral boundary of the model located at 42°S. Past studies, such as *Kousky* [1979], have shown a strong influence of midlatitude frontal systems on the precipitation over northeast Brazil and southeastern South America. The relatively simple land surface

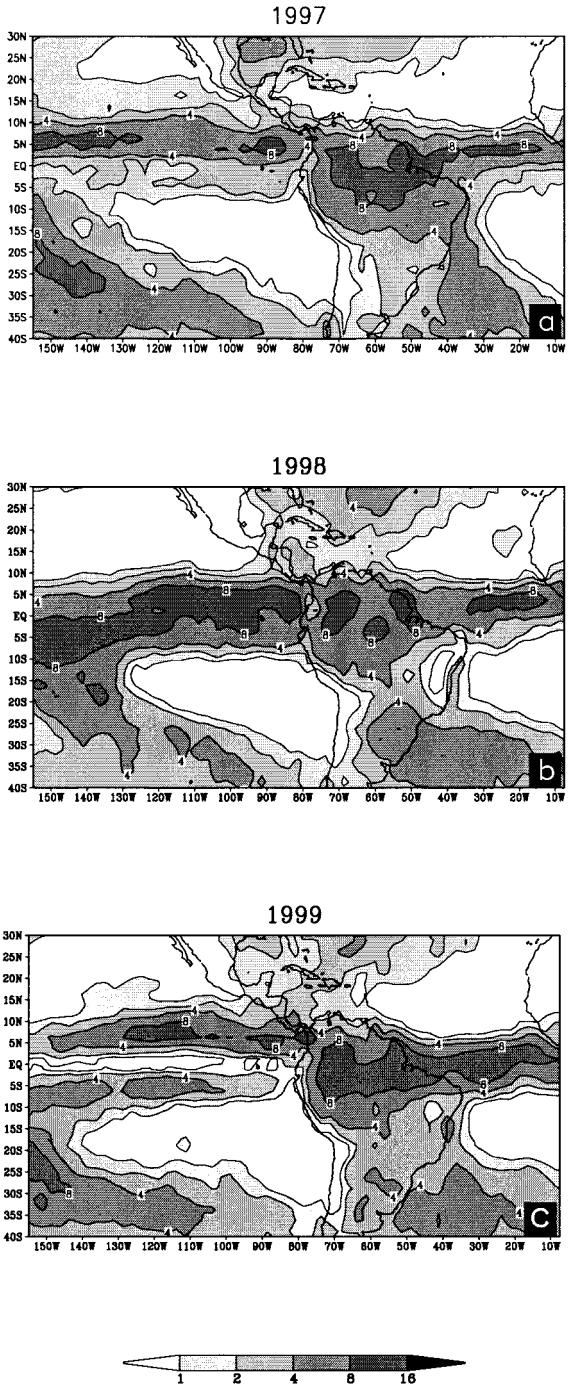

Figure 8. Same as Figure 6 but for the MAM season.

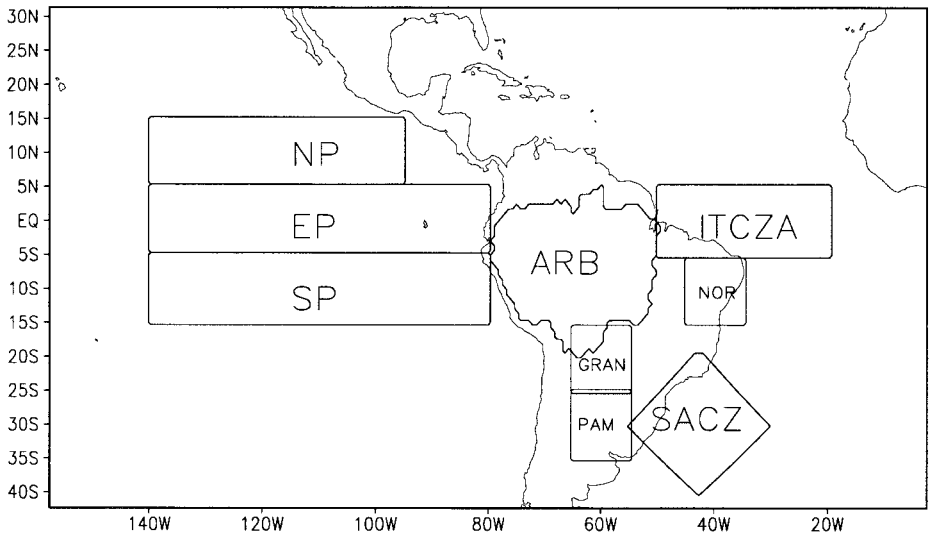

Figure 9. Outline of the Amazon River Basin (ARB), ITCZ over Atlantic (ITCZA), Nordeste (NOR), SACZ, Pampas region (PAM), Gran Chaco area (GRAN), South Pacific (SP), equatorial Pacific (EP), and North Pacific (NP).

scheme also may be a factor in the poor simulation of variability at these frequencies over land.

3.1.2. High-Frequency Variability

[16] In Figures 3a–3c we present the variance of 3 to 30 days-filtered OLR from the RSM, observations, and NCEP reanalysis averaged during JFM 1998. Both the reanalysis and the RSM underestimate the high-frequency variance over the entire region. However, over the Pacific Ocean the broad area of high variance near the equator in the RSM (Figure 3a) compares favorably with observations (Figure 3b), whereas the NCEP reanalysis (Figure 3c) poorly resolves the fine scale features over the equatorial Pacific ocean. Over the Atlantic Ocean and South America the RSM exhibits less variance than both the reanalysis and the observations. However, the simulated spatial structure is coherent with the observations. For example, in the RSM (Figure 3a) the ITCZ in the Atlantic Ocean is discernible as a region of highvariance straddling areas of low variance in the North and South Atlantic Ocean. The observations (Figure 3b) show a similar ITCZ, whereas the NCEP reanalyses (Figure 3c) does not. Likewise, during JFM 1999 (not shown), the improvement over the Pacific Ocean from RSM relative to the NCEP reanalysis is similar to that in the previous year. Low variance over the equatorial Pacific ocean at the equator is better captured by the RSM, but over the North Atlantic, comparison with observations is poor, and the RSM displays very little variance over South America. Similar features in the RSM OLR occurred in JFM 1997 and the MAM seasons in all the 3 years (not shown).

[17] On an average over the 3 years, the RSM simulations display a 15% reduction in the root-mean-square error in OLR at high-frequency scales and about 50% reduction at intraseasonal scales over the NCEP reanalysis.

3.2. Precipitation

3.2.1. Mean Errors

[18] In Figures 4a–4c we show the deviation of RSM JFM precipitation for 1997, 1998, and 1999, respectively, from the 2.5° gridded observed monthly mean values of *Xie and Arkin* [1996]. To make the fields comparable, the model precipitation has been interpolated to the coarser 2.5° grid. In all three figures the positive errors over the northern Andes and Pakaraima Mountains located over north Brazil between 55°W and 70°W are large. These differences are the result of the high-resolution orography used in the model, which induces strong convection from upslope flow. Because of the coarse resolution of the observations, there is a strong possibility that the observations are not able to resolve such features. The errors over the equatorial Pacific Ocean between 5°S and 5°N are less systematic. The model produces more rain than observed in 1997 (Figure 4a), less than observed in 1998 (Figure 4b), and more than observed in 1999 (Figure 4c). Similar errors are also present in the base field (NCEP reanalysis, not shown). This suggests that these errors are carried over by the RSM as a large-scale feature from the reanalysis base field. The precipitation errors over SACZ and extratropical South America are relatively small in comparison. The RSM shows improvement over the NCEP reanalysis precipitation (not shown) over these regions.

3.2.2. Interannual Variability

[19] In Figures 5a–5c the model rainfall is displayed for JFM 1997, 1998, and 1999, and the corresponding observations are shown in Figures 6a–6c. It should be noted that in both as these figures the precipitation is contoured on a exponential scale. The interannual variability of the precipitation over the Pacific ocean, Amazon River Basin (ARB), and the Atlantic Ocean is apparent from the figures. For example, the single (double) ITCZ in the Pacific in 1998 (1999) is nicely simulated by the model (Figures 5b and 5c). Stronger precipitation in the ARB in 1999 (Figure 5c) relative to 1998 (Figure 5b) and 1997 (Figure 5a) is also evident. This feature compares well with observations in Figure 6. Extratropical South America between 20°S and 35°S shows a robust interannual variability with JFM 1998 (Figure 5b), being relatively wet compared to JFM 1998 (Figure 5c), evident from the modulation of the the 8 mm/d contour line. It is found from these model simulations that seasonal mean precipitation (JFM) over this region is reduced

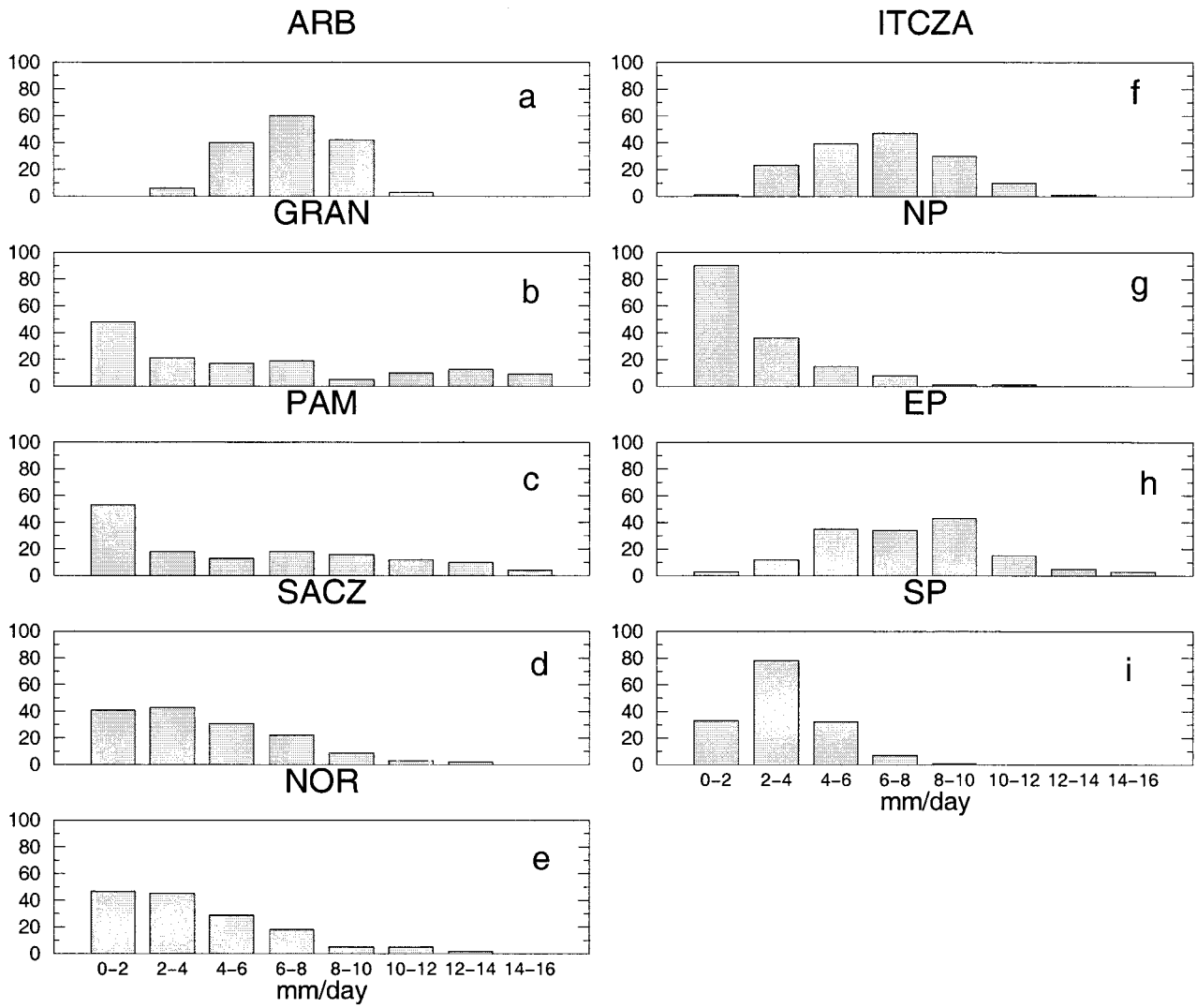

Figure 10. Rainfall distribution over (a) ARB, (b) GRAN, (c) PAM, (d) SACZ, (e) NOR, (f) ITCZA, (g) NP, (h) EP and (i) SP from the 1998, 1999 simulations, respectively. The ordinate denotes number of days.

from 5.9 mm/d in 1998 to 4.4 mm/d in 1999. This feature is also seen in the corresponding observations in Figures 6b and 6c. In an observational study, *Aceituno* [1988] found that in southeastern South America the rainfall tends to be higher than average from November to following February during El Niño years. The variability of precipitation over the SACZ is also well simulated by the model. In 1998 the RSM simulates a broad SACZ with precipitation in excess of 4 mm/d like the observations in Figure 6b. In JFM 1999 the intensity of precipitation in the SACZ is in Figure 5c reduces significantly as the observations indicate in Figure 6c. The RSM also simulates some finescale features, such as the interannual signal over northeast Brazil (southern Nordeste) with rain rates less than 1 mm/d in 1999 relative to 2–4 mm/d in 1997 and 1998, which is in agreement with past observational studies such as *Nobre and Shukla* [1996]. Their study shows that the rainfall composites over southern Nordeste from warm episodes of El Niño exceed the rainfall composites of cold episodes annually by about 200 mm. In addition, the weakening of the northern branch of the ITCZ at around 5°N in 1998 and 1999 over the Atlantic relative to JFM 1997 (Figure 8a) and the amplification of its southern branch (around 5°S) in 1998 are other fine scale features that the RSM has simulated. This is consistent with the warmer SST observed in 1998 in the equatorial Atlantic Ocean (Figure 1).

[20] Figures 7a–7c and 8a–8c illustrate the seasonally averaged rain rates for MAM 1997, 1998, and 1999, from the RSM and observations, respectively. The interannual signal in MAM is weaker over the equatorial Pacific relative to the JFM season in both observations and simulations. Similarly, the RSM captures the interannual variability over subtropical South America reasonably well. The reduction of precipitation in southern South America in 1999 (Figure 7c) relative to 1998 (Figure 7b) is more pronounced than in JFM. This is consistent with *Mechoso and Pêrez* [1992] who identified a clear tendency for the streamflow of the Negro and Uruguay Rivers during June through December to be below average in high southern oscillation index years. Over the Atlantic the RSM simulates the ITCZ with stronger interannual variability. Comparing Figures 7b and 7c, the weakening (strengthening) of the northern (southern) branch at around 5°N (5°S) of the ITCZ from 1998 to 1999 is apparent.

[21] In Figure 9 we outline ARB, the ITCZ over the Atlantic (ITCZA), Nordeste (NOR), SACZ, southern Pampas

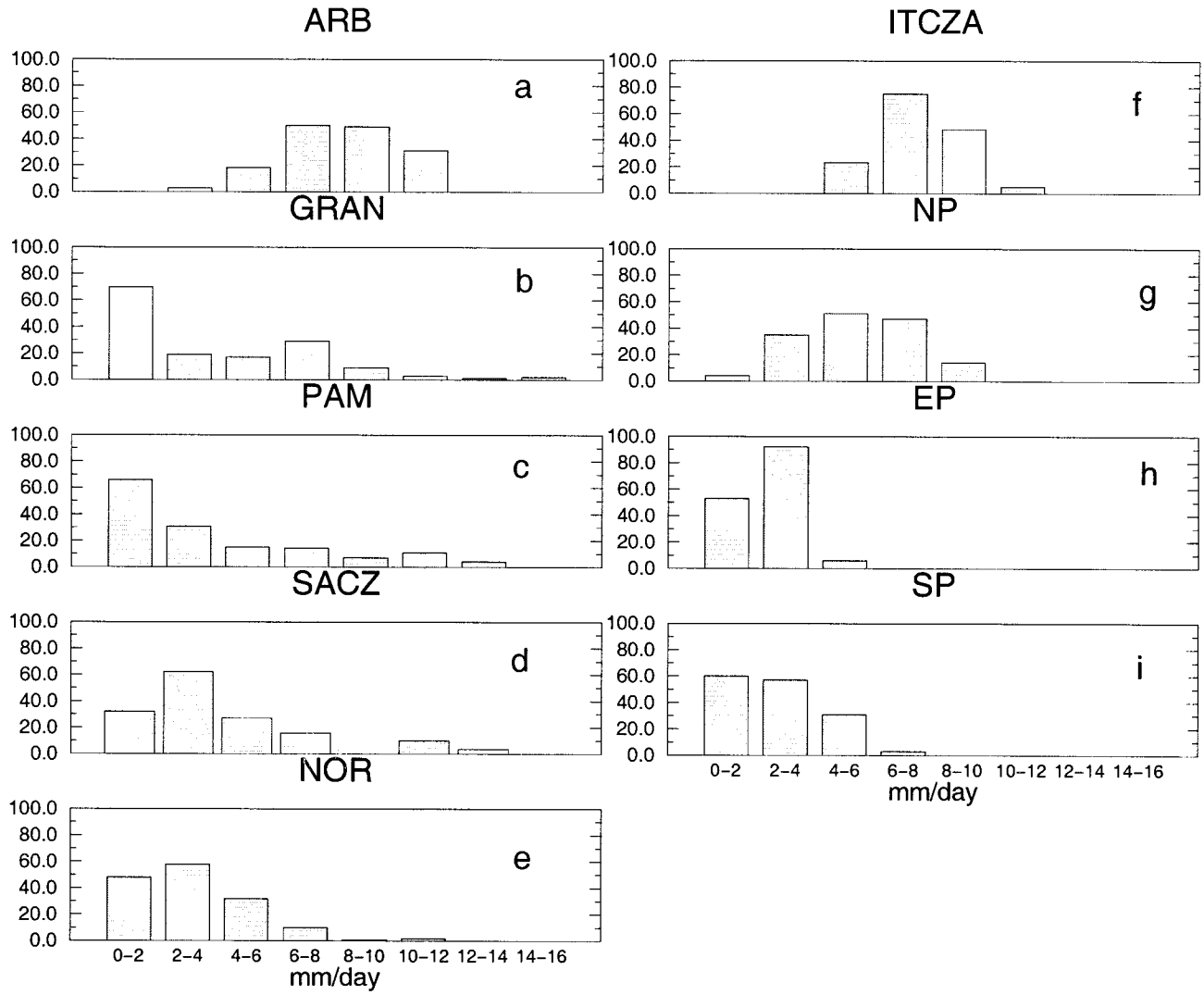

Figure 11. Same as Figure 10 but from the 1999 simulation.

(PAM), Gran Chaco area (GRAN), South Pacific (SP), equatorial Pacific (EP), and North Pacific (NP) for which daily rainfall distributions over the 5 months of integration from January to May will be shown. The daily average precipitation is binned into eight 2 mm/d categories and is shown for 1998 and 1999 in Figures 10 and 11, respectively. Over ARB there is a slight shift of the distribution toward more heavy precipitation events in 1999 relative to 1998. This shift is more apparent over ITCZA and NP as well. In contrast there is a shift toward lower precipitation rates from 1998 to 1999 in NOR, GRAN, PAM, EP, SACZ, and SP. The results from a chi-square test for the significance of the null hypothesis that the precipitation datasets from the two simulations are drawn from the same distribution is shown in Table 1 for all the subdomains. The Chi-square value (χ^2) and the degrees of freedom (DOF) alongside the probability that the observed chi-square will exceed the χ^2 by chance even for a correct model are shown in the table. The large values of χ^2 indicates that the null hypothesis is rather unlikely. Furthermore, the small values of the probability show that there is a significant difference between the two precipitation distributions. Therefore one may conclude that the interannual variability of the simulated precipitation is associated with a change in the number of days of heavy precipitation. In other words, the model simulates changes in "storminess" or the statistics of weather associated with interannual variability.

Table 1. Results of the Chi-Square Test on the Significance of the Null Hypothesis That PDFs of Precipitation From 1998 and 1999 Simulations are Same.[a]

Region	DOF	χ^2	Probability
ARB	4.0	33.85	0.799×10^{-6}
ITCZA	6.0	41.38	0.244×10^{-6}
SACZ	4.0	13.72	0.824×10^{-2}
SP	7.0	226.67	0.00
NP	5.0	138.25	0.00
NOR	6.0	10.37	0.123
PAM	7.0	15.65	0.285×10^{-1}
GRAN	7.0	25.94	0.517×10^{-3}
SACZ	6.0	7.97	0.241

[a]See text for details.

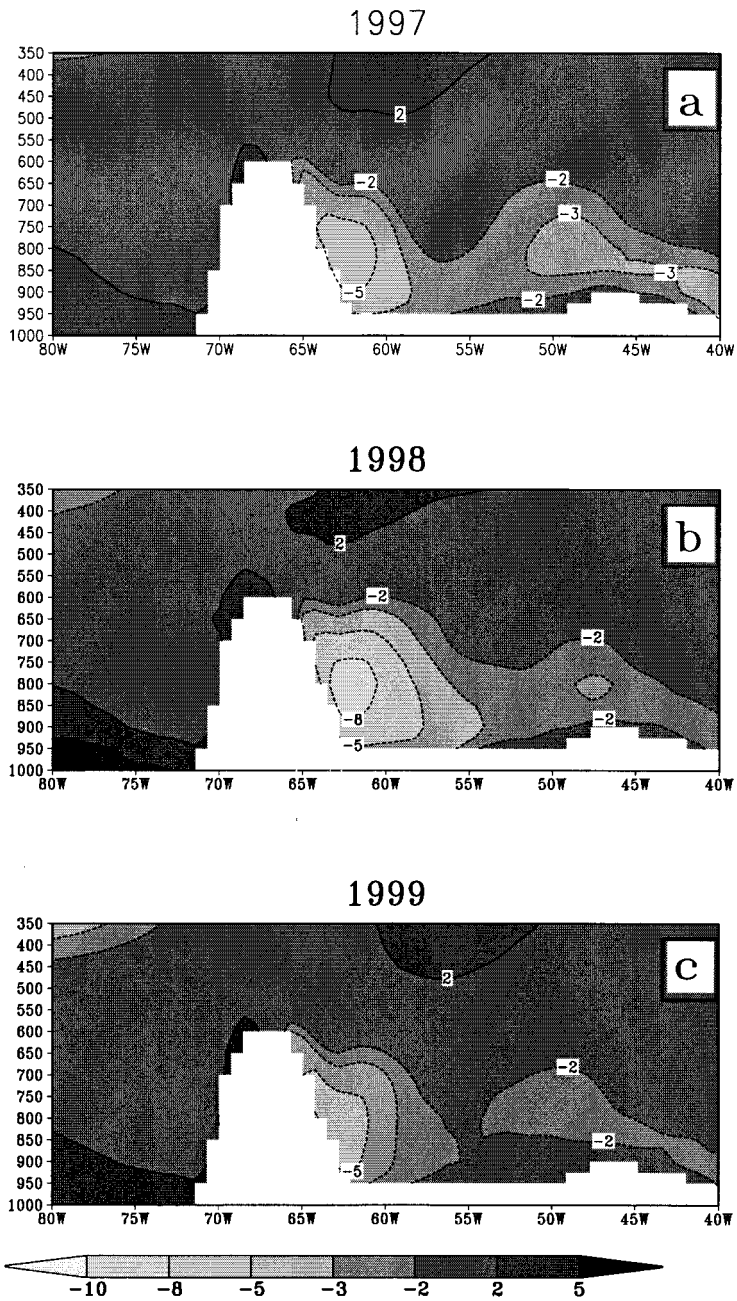

Figure 12 The cross-section of the seasonally averaged (JFM) meridional wind through 20° S in (a) 1997, (b) 1998, and (c) 1999. The units are in m/s.

3.3. Low-Level Jet

[22] In this section we shall discuss the interannual variability of the low level jet (LLJ) east of the Andes and its connection with precipitation in the area. A cross section at 20°S latitude of the seasonally (JFM) averaged meridional wind at 1200 UTC is shown in Figures 12a–12c for 1997, 1998, and 1999, respectively. The amplification of the northerly jet in 1998 is distinct in Figure 12b relative to the other two years. This result is very robust; we examined the cross section of the meridional wind at neighboring latitudes and found similar results. The increased speed of the LLJ in 1998 is consistent with a more intense and westward extending Atlantic subtropical high, which increases the pressure gradient over subtropical South America. This is clearly depicted in Figures 13a–13b which show the JFM 850 hPa geopotential heights for 1998 and 1999, respectively. This more intense and extensive subtropical high in 1998 (Figure 13a) results in a stronger ridge developing into the western part of Brazil almost up to Selvas, thereby increasing the northerlies, while in 1999 (Figure 13b) the subtropical high is weaker and displaced eastward. As a result, there is hardly any noticeable gradient of the geopotential height over central South America.

[23] To understand the relation between the intensity of the LLJ and convection, we defined a jet index as the area-

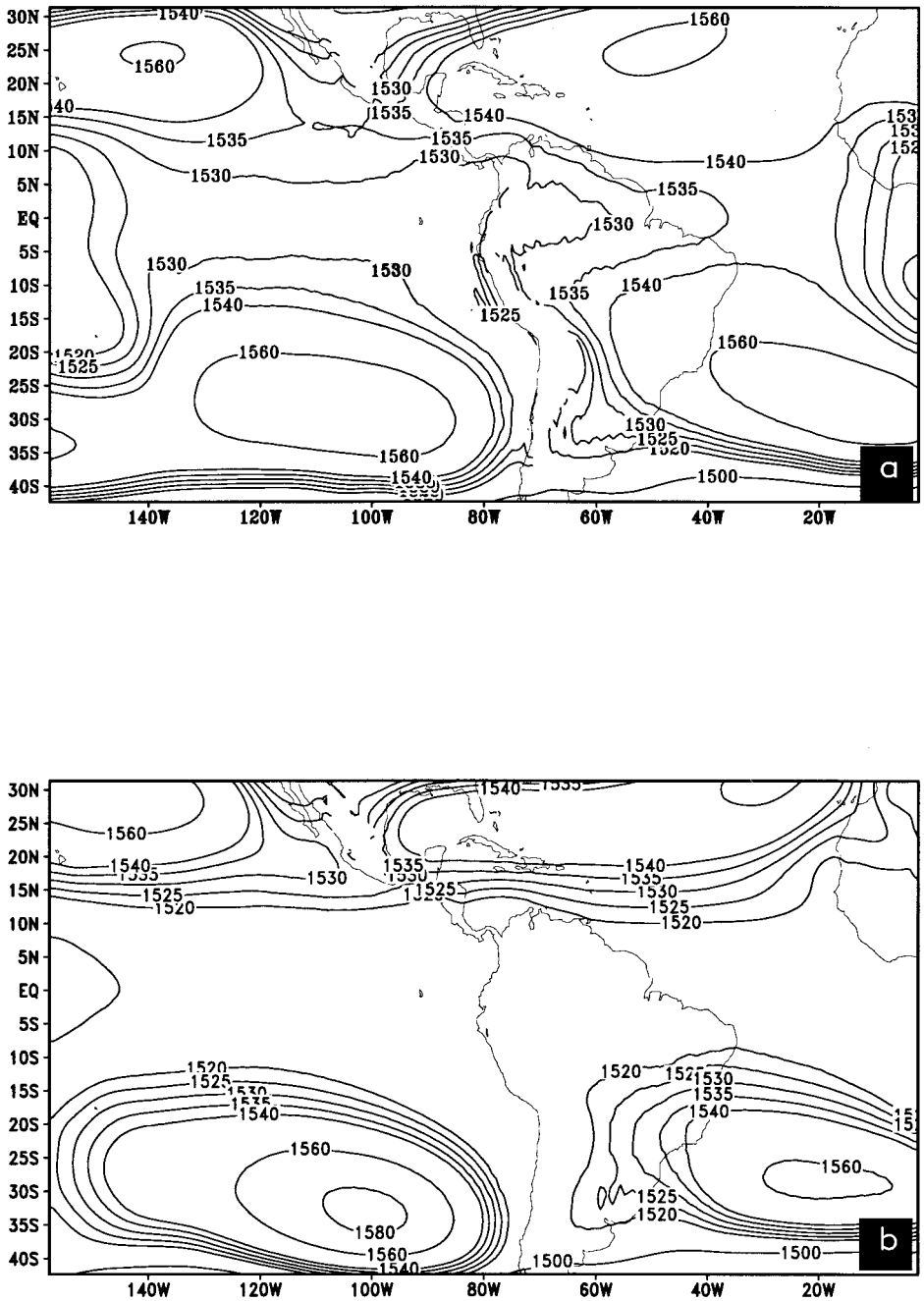

Figure 13. Seasonally averaged (JFM) geopotential heights at 850 hPa for (a) 1998 and (b) 1999 simulations. The units are in meters.

averaged meridional wind over the jet maximum region between 20°S and 17°S latitudes and 63°W and 62°W longitudes at 850 hPa. This index shows an interannual variation similar to that shown in Figure 12. We correlated this jet index at various lag and lead times with precipitation averaged over all areas outlined in Figure 9. We found that the most significant correlations of the jet index were obtained with precipitation over PAM only. This lag correlation is illustrated in Figure 14 for JFM 1997, 1998, and 1999. Here positive lag means that jet index leads the average precipitation. Since the jet index is primarily negative (reflecting that northerlies are negative meridional winds), a strong negative correlation in Figure 14 will suggest that a stronger precipitation over PAM relates to a strengthened jet. The 1% significance level for the correlation coefficient being different from zero using the two-tailed student-*t* test is 0.136. It is clearly seen from the figure that the significant correlations are skewed towards positive lags, indicating that the jet acts as a precursor to precipitation over PAM. This behavior of the LLJ appears to correspond to what is observed in North America, where the jet acts as a conduit to transport water vapor to convective regions at the decelerating edge of the jet.

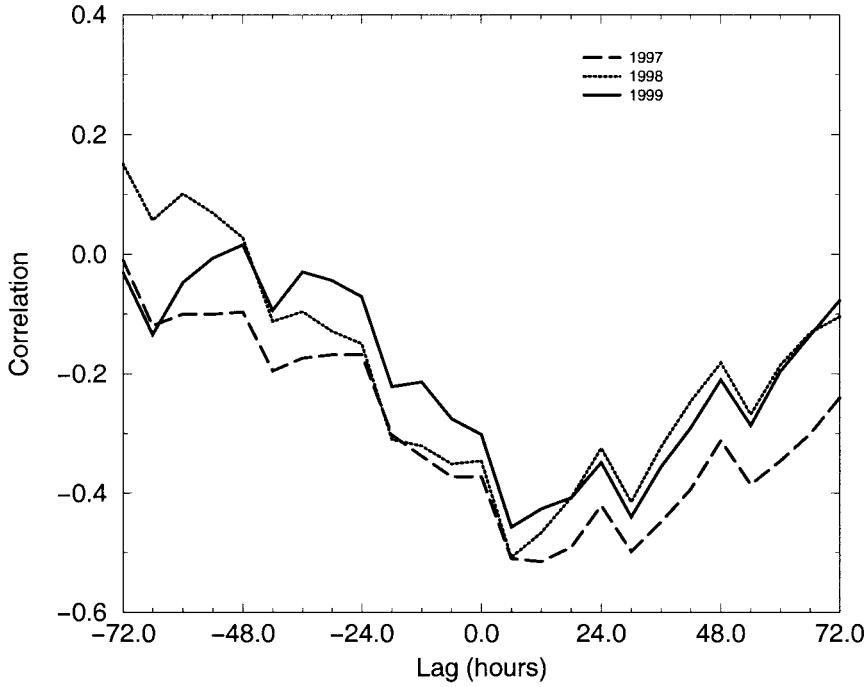

Figure 14. Lag correlation between the jet index and the precipitation averaged over the Pampas region (PAM in Figure 12).

3.4. Moisture Budget

[24] The moisture budget was computed for the regional domains over South America and the Atlantic Ocean outlined in Figure 9 in order to determine the variations in the precipitation sources and sinks and to understand the precipitation variability. In Figures 15–17 the monthly and seasonal moisture budget are illustrated for ARB and GRAN, PAM and SACZ, ITCZA, and NOR from the 1997, 1998, and 1999 simulations, respectively. The storage term (thick solid line in the figures) in the budget is the smallest of all the budget components and shall be ignored in the following discussion. The other components of the budget following the storage term in the figures are moisture flux convergence, precipitation, and surface moisture flux convergence. Moisture flux convergence is obtained as a residue in the budget.

[25] In Figures 15a–15c it is seen that the variations of precipitation over ARB closely follow the moisture flux convergence with surface evaporation being nearly invariant on interannual scales. The increase of 1.55 mm/d in basin average precipitation in JFM 1999 relative to 1998 is consistent with a proportional increase of moisture flux convergence of 2.35 mm/d to 3.63 mm/d. At intraseasonal scales both surface evaporation and moisture flux convergence are also varying comparably. This is evident in all three years of the simulation. Over GRAN, in Figures 14d–14f the variations in precipitation are dependent on both moisture flux convergence and surface evaporation at both intraseasonal and interannual scales. However, at interannual scales the trends are opposite to that seen in ARB, with generally more precipitation in 1998 compared to 1999. Furthermore, the amplitude of variability is much stronger over GRAN. An interesting feature is that the interannual variability of the intraseasonal oscillations in GRAN is very strong. For example, the maximum precipitation of the season in January 1997 shifts to February in 1998 and then nearly becomes equal in January and February 1999.

[26] Like the budget over ARB, that over ITCZA in Figures 16a–16c shows that interannual variability of precipitation is strongely dictated by the moisture flux convergence. Even at intraseasonal scales the moisture flux convergence seems to exert a similar influence over precipitation, although in 1999 the intraseasonal variability of all the budget components is very small relative to the other two years shown in the figure. Over NOR (Figures 16d–16f), the moisture flux convergence is clearly the important forcing for the variability of precipitation at both intraseasonal and interannual scales.

[27] The budget over PAM in Figures 17a–17c indicates that the interannual and intraseasonal variation of precipitation is equally derived from the corresponding variations in moisture flux convergence and surface evaporation. Similar to the budget over GRAN, PAM also exhibits relatively smaller interannual variation in the seasonal mean of JFM and MAM. However, there is a considerable interannual variation of the moisture budget components from month to month. In other words the interannual variability of the intraseasonal variation is significant. The budget over SACZ in Figures 17d–17f indicates that unlike ITCZA, surface evaporation and moisture flux convergence both play a decisive role in the interannual and intraseasonal variation of precipitation over the region. Furthermore, there is a larger interannual variability of precipitation over SACZ in both JFM and MAM seasons between 1997 and 1999 compared to 1998 and 1999. This result is consistent with the larger Atlantic SST variability between 1997 and 1999 pointed out in the introduction.

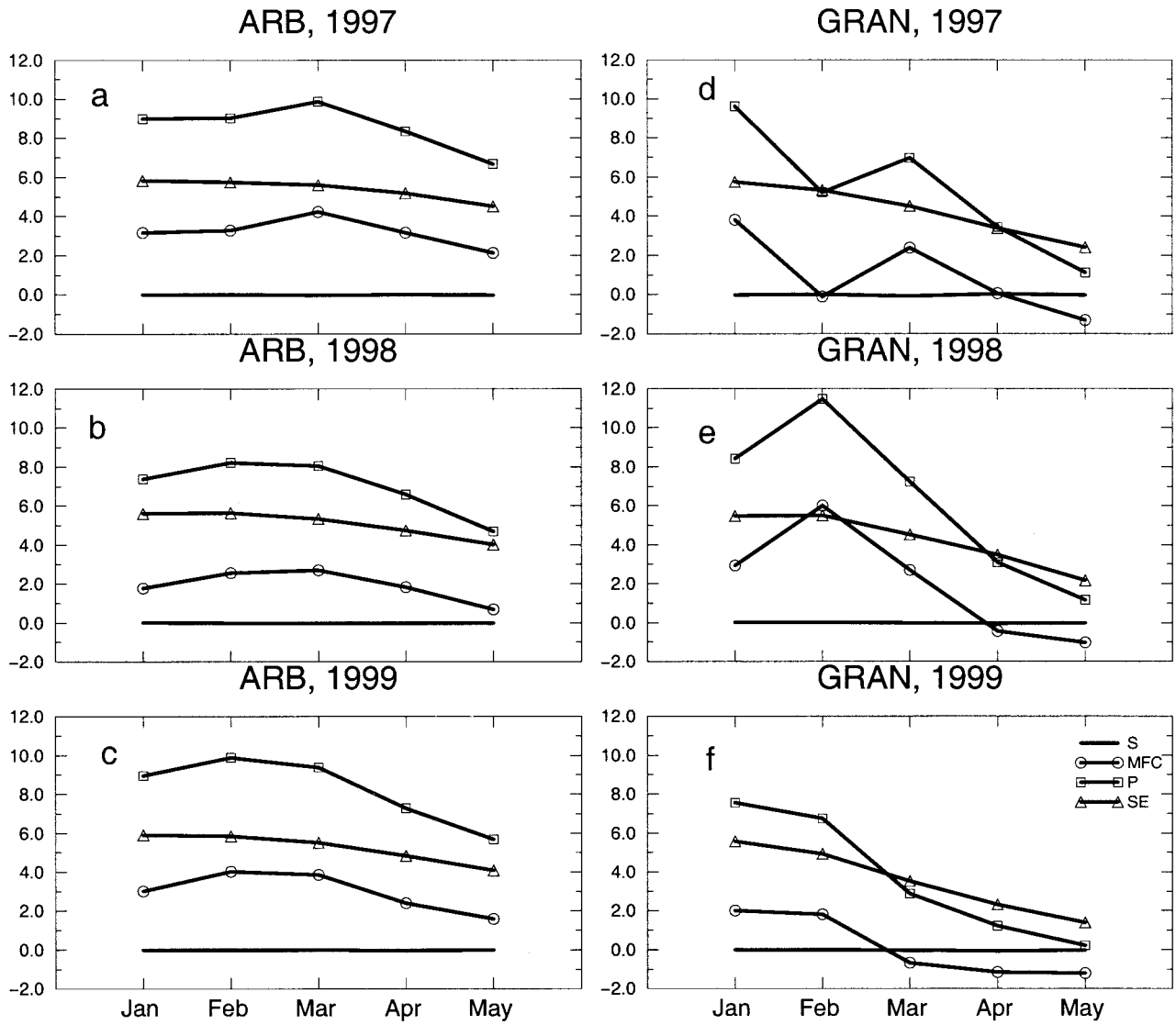

Figure 15. The moisture budget over the ARB and GRAN (see Figure 9) (a, d) 1997, (b, e) 1998 and (c, f) 1999 simulations. The units are in mm/d. The moisture budget components are storage (S), moisture flux convergence (MFC), precipitation (P) and surface evaporation (SE).

[28] It is worth noting here that the connection between the LLJ and precipitation over PAM is apparent from this budget study. The excess precipitation over this region in 1998 relative to 1999 comes from increased moisture flux convergence in the area in 1998 when the jet reaches its maximum. *Paegle and Mo* [1997] have shown that increase in moisture flux in the subtropical South America during wet episodes is largely from a more intense LLJ.

4. Conclusions

[29] We have conducted three climate simulations of 5 months duration centered over South America using the Regional Spectral Model (RSM) during contrasting states of the sea surface temperature over the Pacific Ocean basin. The RSM optimally filters the perturbations about a time-varying base field, thereby, enhancing the information content of the base field.

[30] The impact of the higher resolution of the RSM relative to NCEP reanalysis is easily discernible at high frequency and intraseasonal scales. The simulated outgoing longwave radiation (OLR) shows significant improvements over the NCEP reanalysis in explaining the variance at these scales over both the Pacific and the Atlantic Ocean basins. Furthermore, it is able to discern the South Atlantic Convergence Zone (SACZ) and ITCZ over the Atlantic, while the NCEP reanalysis failed to resolve these features adequately. However, the RSM does exhibit some limitations, such as in producing far lower variance in OLR than observed over SACZ and the North Atlantic. This may be due to the inability of the RSM to adequately capture the influence of the intrusions of the midlatitude frontal systems due to the extent of the model domain in the north-south direction.

[31] The RSM shows reasonable skill in capturing the interannual variability of the precipitation over the ITCZ in the Pacific and the Atlantic Ocean basins and over the

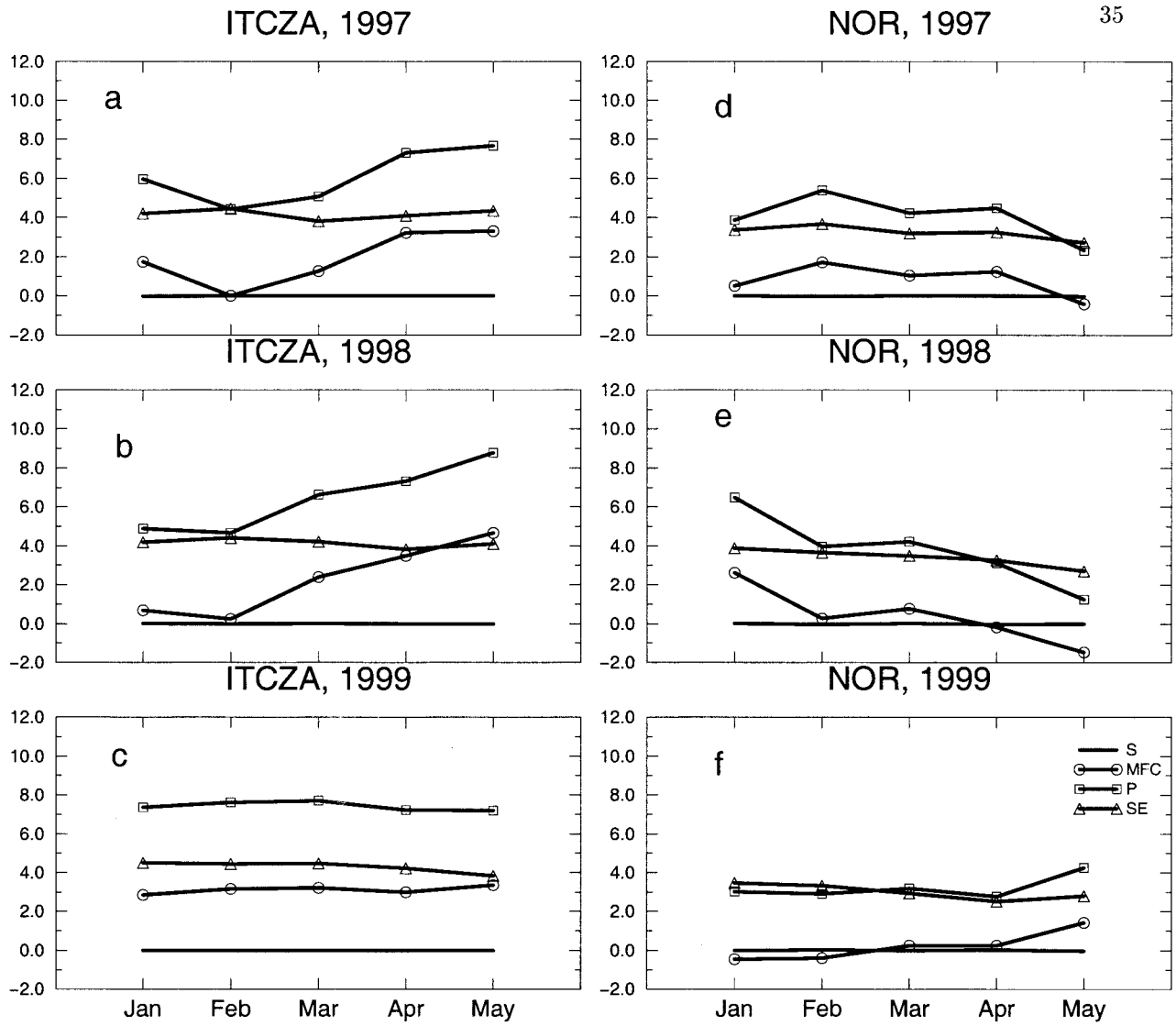

Figure 16. Same as Figure 15 but over ITCZA and NOR.

Amazon River Basin (ARB). Regionally, the interannual variability over southern Nordeste and over extratropical South America conforms to the past observational work. The rainfall distribution indicates that variability of storminess from one year to the other is important for the simulation of the interannual variability of the precipitation over these regions. This emphasizes the necessity to conduct climate modeling studies at higher spatial and temporal resolutions. Insights into the interannual variability of the low level jet (LLJ) is an important aspect revealed by higher-resolution simulations. The amplitude of the LLJ is closely linked to variations in the subtropical high over the Atlantic. The jet acts as a precursor to convection over Pampas, similar to the LLJ of North America, where convection outbreaks at the decelerating edge of the jet are common. However, besides this relationship, the jet did not have a statistically significant relationship with convection over other regions. These features remain to be confirmed from observations.

[32] The moisture budget study revealed the importance of the moisture flux convergence and surface evaporation to the variability of precipitation at interannual and intraseasonal scales. It was apparent from the simulations that the intraseasonal variability is more robust in the subtropical regions of GRAN, PAM and SACZ regions. In addition, the interannual variability of precipitation over ITCZA and SACZ is more critically dependent on the Atlantic SST variability. It is observed that the original NCEP reanalysis has a dry bias in soil moisture (J. Roads, personal communication, 2000). Preliminary results using NCEP reanalysis-2 for regional climate simulations, which has a larger interannual variability of soil moisture, indicate that surface evaporation plays a more important role in the moisture budget over the region.

[33] The model has its limitations. The foremost in this study is probably the simplistic nature of the land surface scheme which does not consider the spatial heterogeneity in vegetation and soil types. We are at present conducting

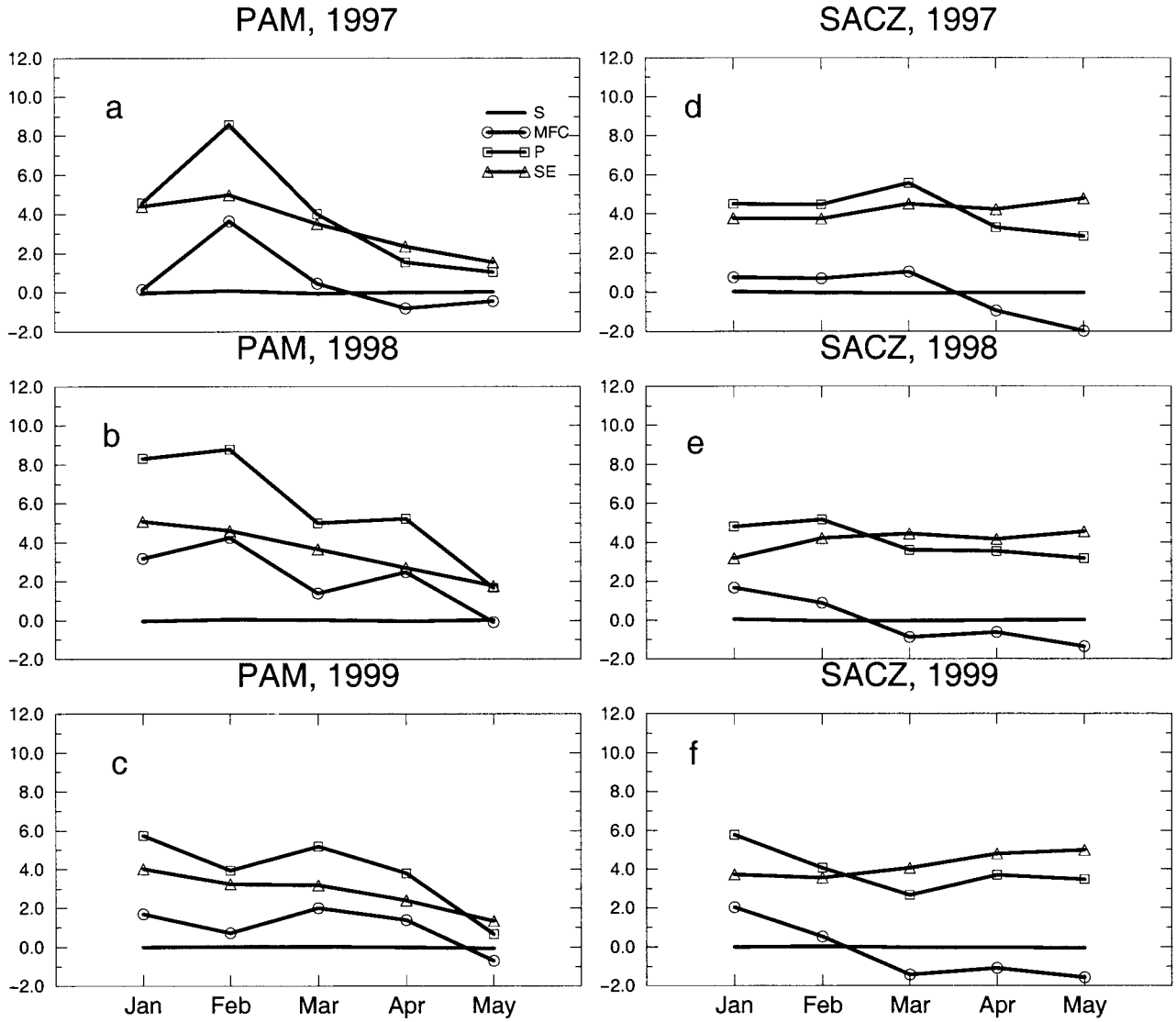

Figure 17. Same as Figure 15 but over PAM and SACZ.

similar seasonal regional climate simulations with a more sophisticated coupled land-atmosphere model. The results from these integrations will be presented in a future paper. Nonetheless, the model simulations in this study shed light on some of the fine scale features not revealed in the coarser analysis and observations. This is useful particularly over the data-void regions such as the tropical rain forest area over the ARB.

[34] **Acknowledgments.** We thank Mike Fennessey for his very useful comments which substantially improved this paper. We also thank Eric L. Altshuler for helping us in preparing the initial conditions. We would like to thank the Climate Diagnostics Center for providing us the Fortran code for the spectral filter, and M. G. Logsdon of the College of Ocean and Fishery Sciences, University of Washington, for providing us the mask for the Amazon River Basin. This project was supported by NASA grant NAG5-8416 as part of The Large-Scale Biosphere-Atmosphere Experiment in Amazonia (LBA), and NOAA grant NA86GP0258.

References

Aceituno, P., On the functioning of the Southern Oscillation in the South American sector, Part I, Surface climate, *Mon. Weather. Rev., 116,* 505–524, 1988.

Alpert, J. C., M. Kanamitsu, P. M. Caplan, J. G. Sela, G. H. White, and E. Kalnay, Mountain induced gravity wave drag parameterization in the NMC medium range forecast model paper presented at Eighth Conference on Numerical Weather Prediction, Baltimore, Md., 1988.

Chou, M.-D., A solar radiation model for use in climate studies, *J. Atmos. Sci., 49,* 762–772, 1992.

Fels, S. B., and M. D. Schwarzkopf, The simplified exchange approximation, A new method for radiative transfer calculations, *J. Atmos. Sci., 37,* 2265–2297, 1975.

Grimm, A. M., V. R. Barros, and M. E. Doyle, Climate variability in southern South America associated with El Niño and La Niña events, *J. Clim., 13,* 35–58, 2000.

Hong, S.-Y., and H.-L. Pan, Nonlocal boundary layer vertical diffusion in a medium-range forecast model, *Mon. Weather Rev., 124,* 2322–2339, 1996.

Juang, H.-M., and M. Kanamitsu, The NMC nested regional spectral model, *Mon. Weather Rev., 122,* 3–26, 1994.

Juang, H.-M., S.-Y. Hong, and M. Kanamitsu, The NCEP regional spectral model: An update, *Bull. Am. Soc., 78,* 2125–2143, 1997.

Kousky, V. E., Frontal influences on northeast Brazil, *Mon. Weather. Rev., 107,* 1140–1153, 1979.

Liebmann, B., and C. A. Smith, Description of a complete (interpolated) outgoing longwave radiation dataset, *Bull. Am. Soc., 77,* 1275–1277, 1996.

Liebmann, B., G. N. Kiladis, J. A. Marengo, T. Ambrizzi, and J. D. Glick, Submonthly convective variability over South America and the South Atlantic Convergence Zone, *J. Clim., 12,* 1877–1891, 1999.

Lenters, J. D., and K. H. Cook, Summertime precipitation variability over South America: Role of the large-scale circlation, *Mon. Weather. Rev., 127,* 409–431, 1999.

Mahrt, L., and H.-L. Pan, A two layer model of soil hydrology, *Boundary. Layer Meteorol., 29,* 1–20, 1984.

Marengo, J. A., and S. Hastenrath, Case studies of extreme climatic events in the Amazon Basin, *J. Clim., 6,* 617–627, 1993.

Mechoso, C. R., and G. Perez-Iribarren, Streamflow in southeastern South America and the Southern Oscillation, *J. Clim., 5,* 1535–1539, 1992.

Mohr, K. I., and E. J. Zipser, Mesoscale convective systems defined by their 85-GHz ice scattering signature: Size and intensity comparison over tropical oceans and continents, *Mon. Weather. Rev., 124,* 2417–2437, 1996.

Nobre, P., and J. Shukla, Variations of sea surface temperature, wind stress, and rainfall over the tropical Atlantic and South America, *J. Clim., 9,* 2464–2479, 1996.

Paegle, N., and K. C. Mo, Alternating wet and dry conditions over South America during summer, *J. Clim., 125,* 279–291, 1997.

Pan, H.-L., A simple parameterization scheme of evapotranspiration over land for the NMC medium-range forecast model, *Mon. Weather. Rev., 118,* 2500–2512, 1990.

Pan, H.-L., and L. Mahrt, Interaction between soil hydrology and boundary layer developments, *Boundary Layer Meteorol., 38,* 185–202, 1987.

Pan, H.-L., and W.-S. Wu, Implementing a mass flux convective parameterization package for the NMC medium-range forecast model, *NMC Off. Note 409,* 40 pp., Natl. Meteorol. Cent., Camp Springs, Md., 1995. (Available from NOAA/NWS/NCEP, Environ. Model. Cent., WWB, Washington, D.C.)

Pisciottano, G., A. Diaz, G. Caszes, and C. R. Mechoso, El Niño-Southern Oscillation impact on rainfall in Uruguay, *J. Clim., 7,* 1286–1302, 1994.

Reynolds, R. W., and T. M. Smith, Improved global sea surface temperature analyses using optimum interpolation, *J. Clim., 7,* 929–948, 1994.

Ropelewski, C. F., and M. S. Halpert, Global and regional scale precipitation patterns associated with the El Niño-Southern Oscillation, *Mon. Weather. Rev., 115,* 1606–1626, 1987.

Rullant, J., and H. Fuenzalida, Synoptic aspects of the central Chile rainfall variability associated with the Southern Oscillation, *Int. J. Climatol., 11,* 63–76, 1991.

Tiedtke, M., The effect of penetrative cumulus convection on the large-scale flow in a general circulation model, *Beitr. Phys. Atmos., 57,* 216–239, 1984.

Uvo, C. B., C. A. Repelli, S. E. Zebiak, and Y. Kushnir, The relationships between tropical Pacific and Atlantic SST and Northeast Brazil monthly precipitation, *Mon. Weather. Rev., 11,* 551–562, 1998.

Xie, P., and P. Arkin, Analysis of global monthly precipitation using guage observations, satellite estimates, and numerical model predictions, *J. Clim., 9,* 840–858, 1996.

P. A. Dirmeyer, B. P. Kirtman, and V. Misra, Center for Ocean-Land-Atmosphere Studies, Institute of Global Environment and Society, Inc., 4041 Powder Mill Road, Suite 302, Calverton, MD 20705, USA. (dirmeyer@cola.igcs.org; kirtman@cola.iges.org; misra@cola.iges.org)

H.-M. H. Juang, National Centers for Environmental Prediction, Climate Prediction Center, Camp Springs, MD 20746, USA. (wd20hh@ncep.noaa.gov)

M. Kanamitsu, Climate Research Division, Scripps Institution of Oceanography, University of California, San Diego, La Jolla, CA 92093, USA. (kana@ucsd.edu)